Received: April 13, 2025. Revised: May 20, 2025.

International Journal of
Intelligent Engineering & Systems

http://www.inass.org/

AI-Based Hybrid Control for Optimizing Doubly-Fed Induction Generators in Wind Turbines

Samir Abood[1] **Annamalai Annamalai**[1] **Islam Khalid**[2] **Mohamed Chouikha**[1]
Huda Abbood Al-Zuhairi[3]

[1]Electrical and Computer Engineering Department, College of Engineering, Prairie View A&M University, USA
[2] Electric Power and Machine Department, College of Engineering, University of Diyala, Iraq
[3]University of Texas Rio Grandy Valley
* Corresponding author's Email: siabood@pvamu.edu

Abstract: Transitioning to sustainable alternatives, such as Wind Energy Conversion Systems (WECS), provides an eco-friendly and cost-effective solution. Due to technological advancements, WECS has become increasingly reliable. A new variable-speed wind energy conversion approach utilizes a wound-rotor asynchronous machine called the Doubly Fed Induction Generator (DFIG). This machine is operated by an Alterable-Speed Wind Turbine (ASWT) that uses an advanced power electronic converter design. While DFIG-based configurations offer significant advantages in reducing energy costs, they also present issues related to grid integration, power quality, frequency, and voltage fluctuations, among other concerns. This paper aims to develop an optimized design for DFIG and a corresponding control system necessary for advancing renewable energy progress based on Artificial Intelligence (AI). The research focuses on fine-tuning DFIG design by evaluating varying parameters, such as stator resistance and slot numbers, and its operational behavior at different speeds. Importance is placed on ensuring that the DFIG operates within its designated speed, torque, and power ratings by utilizing pitch angle control to adjust for variations in wind speed. A hybrid approach integrating Proportional-Integral (PI) control and an Adaptive Neuro-Fuzzy Inference System (ANFIS) is proposed to enhance the vector control mechanism using dual converters in a DFIG. The novel idea of this work is to intelligently combine artificial intelligence algorithms such as ANFIS and Fuzzy Logic (FLC) with the Particle Swarm Optimization (PSO) algorithm. This control was implemented on a realistic simulation system using Lucas-Nülle laboratory equipment, resulting in improved response speed, reduced total harmonic distortion (THD), and increased performance efficiency compared to traditional methods. Simulation and modeling results showed that using the PSO-ANFIS algorithms reduced the settling time to 0.16 seconds and reduced the total harmonic distortion (THD) to 0.9%, compared to the conventional PI method, which recorded a settling time of 0.72 seconds and a distortion of 4.21%.

Keywords: ANFIS, APSO, DFIG, FLC, Hybrid control, Optimizing wind turbines, WECS.

1. Introduction

Due to its many advantages, DFIG is the preferred choice for the most significant wind energy systems. These advantages include the ability to control and respond to power independently, reduced flicker, maximum control over generation despite variations in wind speed, and a low initial investment. Additionally, the rotor speed of a DFIG can be regulated to transition between sub-synchronous and

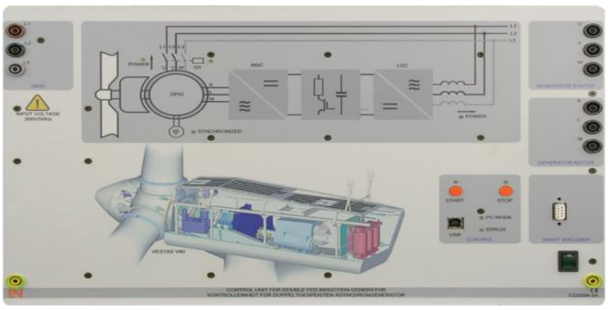

Figure. 1 General schematic of DFIG [2]

Received: April 13, 2025. Revised: May 20, 2025.

super-synchronous operation. [1] . Fig. 1 shows a general schematic of a typical DFIG system used in this work. [2].

This type of induction device has a wound rotor. Because DFIG's stator and rotor windings are connected to the electric grid, the term "doubly fed" is appropriate. When the stator windings intended for DFIG are connected directly to the grid, while the rotor windings are linked to bi-directional power converters. A DFIG-based wind system is more efficient than other wind power generators, making it a viable option for grid-connected Variable-Speed Wind Turbines (VSWT) [3].

This study focuses on a DFIG-based VSWT for wind power applications, which leverages the numerous benefits of the DFIG machine. [4, 5].

In this paper, we regulate the actual power necessary for optimal operating points. Capturing peak wind energy and maintaining precise power regulation during severe wind conditions. The reactive power of the flow in a DFIG can be managed and introduced between the value grid and it, paying particular attention to weaker grid connections where voltage swings occur. Low-voltage ride-through (LVRT) ability is mandatory in many power grids, requiring wind turbines to remain connected even during brief voltage drops.

The primary objectives of this endeavor are: (i) Design a DFIG using a stationary reference frame and investigate the impact of parameters on DFIG's performance when connected to a wind turbine system. (ii) Design and simulate the back-to-back converter and the power flow through these converters, focusing primarily on reactive power in the DFIG and the primary grid, utilizing Artificial Intelligence. (iii) Enhance grid and rotor-side control to achieve optimal performance of the DFIG in a wind turbine system.

This work integrates AI algorithms (ANFIS and FLC) with PSO to tune controllers in a realistic simulation environment using Lucas-Nülle equipment, achieving improvements in reducing settling time, reducing harmonics, and increasing power generation efficiency under variable wind conditions, which previous works have not comprehensively covered. This research proposes a comprehensive design for DFIG wind turbines, including an investigation into the impact of manufacturing parameters on power flow during the back-to-back conversion phase. The proposed design is based on fuzzy logic and ANFIS controllers, with a pitch angle manager, to prevent the DFIG from exceeding its rated speed, torque, and power. What distinguishes this work from previous studies is the intelligent integration of three control techniques within a single framework. A PI controller tuned using the PSO algorithm was combined with two advanced control systems: FLC and ANFIS. The PSO algorithm dynamically optimizes the PI parameters to achieve better control performance. The FLC and ANFIS handle nonlinear conditions and sharp speed changes. This unique approach uses an intelligent supervisory unit that selects the most appropriate controller output based on fault conditions and speed. This adaptive switching has not been documented in detail in previous literature using this combined configuration. Furthermore, the system was implemented on a Lucas-Nülle platform for real-time testing, enhancing this work's practical contribution. Thus, this research combines algorithmic optimization, intelligent adaptation, and real-time experimental verification. This research is divided into several sections: Section 2 reviews the literature on DFIG systems using artificial intelligence. Section 3 explains the proposed design and modeling methodology. Section 4 presents the mathematical models used. Section 5 presents the simulation, control, and analysis results. Section 6 concludes with conclusions and findings.

2. Literature review

Recent studies on DFIG using wind energy conversion Systems (WECS) have focused on enhancing performance through various advanced control techniques. Sayeh et al. [6] used two intelligent DFIG control networks, PNN-DPC and CNN-DPC, to improve the quality of active and reactive power, reducing power ripples by more than 72% and improving current quality (THD less than 2.5%). Zhang et al. [7] developed a technique to optimize speed and frequency responses in wind systems using an ANN implemented in predictive direct control, achieving a 35% reduction in response time compared to SMC. Lin et al. [8] proposed a hybrid strategy based on FLC and PSO to adjust DFIG control to wind changes, improving dynamic tracking and reducing static error in the generated power. Rajendran et al. [9] presented an adaptive AI-based model using DNNs for power management and voltage generation in DFIG systems. The method achieved a 65% reduction in power losses compared to classical control. Dardabi et al. [10] used a deep learning-based controller to improve the stability of a WT-DFIG system under sudden wind changes, and the results showed a significant improvement in reducing electromechanical speed fluctuation and reducing power losses by 65% compared to conventional control. Li X et al. [11] A fuzzy sampled data control DFIG-based WECS was used, and improved fault tolerance was applied. Renzeng et al. [12] utilized AI-based harmonic load identification for distribution networks, enhancing identification accuracy. Sayeh et al. [13] developed an AI-based direct power control for the WT-DFIG system, enhancing power quality. Ma et al. [14] use the Bayesian Ensemble Kalman Filter by DFIG for enhanced dynamic state estimation.

Sreenu et al. [15] Utilizing Quasi Z-Source Converters for enhanced power conversion in solar-wind energy systems. Further advancements include Loulija et al. [16], who introduced the Backstepping in Nonlinear Control approach to DFIG-based wind energy conversion systems (WECS), enhancing low-voltage ride-through (LVRT) capability. Sanati et al. [17] Have improved inrush current detection in DFIG-based wind farms for enhanced differential protection. In earlier contributions. The current study presents an AI-based hybrid control approach that integrates ANFIS, fuzzy logic, and PSO-based PI control for real-time DFIG-based WECS, optimizing system stability, efficiency, and adaptive response under varying conditions. Table 1 shows the studies related to DFIG-based WECSs.

Although many previous studies have used conventional simulation environments to study the performance of DFIG, there is an apparent lack of studies that rely on real-time simulation using systems such as Lucas-Nülle (LN). Therefore, this research aims to fill this gap by integrating the MATLAB/Simulink simulation environment with the LN system to study the performance of DFIG

Table 1. The related studies of DFIG-based WECSs

Researchers	**Year**	**Technology Used**	**System model**	**Results**
Sayeh et al.	2025	PNN-DPC & CNN-DPC (AI)	WT-DFIG	Reduce active and reactive power ripples by over 72%, and THD to less than 2.5%
Liu et al.	2025	FLC + PSO Hybrid Strategy	DFIG under wind change	Improve dynamic tracking and reduce static error in output power.
Xiaoqing et al.	2025	Fuzzy Sampled-Data Control	DFIG-Based WECS	Improved fault tolerance
Yang et al.	2025	AI-Based Harmonic Load Identification	Distribution Networks	Enhanced identification accuracy
Karim et al.	2025	AI-Based Direct Power Control	WT-DFIG System	Enhanced power quality
Wentao et al.	2025	Bayesian Ensemble Kalman Filter	DFIG	Enhanced dynamic state estimation
Sreenu et al.	2025	Quasi Z-Source Converters	Solar-Wind Energy	Enhanced power conversion
Azeddine et al.	2025	Nonlinear Backstepping Control	DFIG-Based WECS	Enhanced LVRT capability
Zhang et al.	2024	ANN + Predictive Direct Control	Wind Turbine (WT)	Improved speed and frequency response with 35% reduced response time compared to SMC
Hassan et al.	2024	MPC + PSO Hybrid Control	WT-DFIG	Improved active power by 93.75% and reduced THD by 67.81%.
Ahmed et al.	2024	Adaptive DNN-based Control	DFIG	Reduce power losses by 65% compared to conventional control
Dardabi et al.	2024	ANN	WT-DFIG with real wind profiles	Improved control accuracy and output stability under real wind disturbances
Prasanna et al.	2024	CNN-Based Power Distribution	DC/AC Microgrids	Optimized power flow
Saeed et al.	2023	Inrush Current Detection	DFIG-Based Wind Farms	Improved differential protection
Younes et al.	2023	DTC Analysis	WT-DFIG System	Improved switching strategy
Jinfeng et al.	2023	AI & Wind Power	Patent Analysis	Insights into tech interactions
Saeed Sanati, Maher Azzouz	2023	Differential Protection	DFIG-Based Wind Farms	New inrush current detection
This study	2025	AI Technologies ANFIS, Fuzzy based on PI and PSO	Real-time DFIG-Based WECS	Optimized DFIG design, improved AI-based control, enhanced system stability

Received: April 13, 2025. Revised: May 20, 2025.

under various operating conditions, providing more accurate and realistic results than conventional simulation.

Although many previous studies have employed intelligent control techniques, such as ANFIS and FLC, in doubly fed induction generator (DFIG) systems, this research improves by integrating these techniques with a real-time simulation system utilizing the LN system. This allows for more realistic testing and more accurate analysis of system performance. In addition, the control is enhanced by incorporating adaptive AI techniques, resulting in more stable performance and faster response times compared to previous studies. The results demonstrate that this improved methodology leads to reduced oscillation and improved integration with the grid.

This research differs from previous studies by presenting an integrated approach that combines adaptive fuzzy control (ANFIS) with the optimization of control parameters using a particle swarm optimization (PSO) algorithm.

The research also utilizes a real-time simulation platform that analyzes performance under various operating conditions in DFIG, enabling a more accurate evaluation than conventional simulation methods. These innovations contribute to achieving more stable control and higher efficiency in generator-grid interaction.

3. Methodology

DFIG control strategies play a central role in optimizing the performance of wind energy systems. They enable precise manipulation of the generator's rotor currents, directly impacting the active and reactive power output. Table 2 presents the list of notations used in this paper and their definitions.

3.1 Design and modeling of DFIG-fed wind turbine

This work presents an optimal DFIG wind turbine system design based on grid-connected back-to-back converters. Its main contribution is introducing a complete design for DFIG and controller system-based wind systems. The DFIG wind turbine has a closed-loop control system model. The decoupling vector control approach is practical across all converters, including the rotor and the grid. The PI controller parameter is adjusted using a PSO algorithm to attain optimal performance under varying wind speeds. A 2MW large-scale wind generator system is available to validate the proposed design. Fig. 2 illustrates the system configuration.

Table 2. Notations, definitions, and unit

Notation	Definition	Unit
$dt/d\omega_r$	Rate of change of rotor speed	rad/s²
$dt/d\theta$	Rate of change of twist angle of the shaft	rad/s
$dt/d\omega_t$	Rate of change of turbine speed	rad/s²
H_g	Generator's inertia constant	sec
H_t	Turbine's inertia constant	sec
T_{sh}	Shaft torque	Nm
T_e	Electromagnetic torque	Nm
B	Damping constant	Nm/(rad/s)
ω_b	Base speed	rad/s
ω_r	Rotor speed	rad/s
ω_t	Turbine speed	rad/s
T_m	Mechanical torque	Nm
L_m	Mutual inductance	Henry (H)
i_{qs}	Q-axis stator current	Amperes
i_{dr}	D-axis rotor current	Amperes
i_{ds}	D-axis stator current	Amperes
i_{qr}	Q-axis rotor current	Amperes
K_{sh}	Shaft stiffness constant	Nm/rad
D_{sh}	Shaft damping constant	Nm/(rad/s)
ω_{ref}	Reference rotor speed	rad/s
K_{opt}	Optimal torque constant	Nm
λ_i	Adjusted tip speed ratio	Unitless
Ω/Ω_t	Turbine angular velocity	rad/s
R	Rotor radius	Meters (m)
E	Kinetic energy of the moving air particles	Joules (J)
m	Total mass of the air particles	kg
V_W	Air particles' velocities	m/s
ρ	Air density	kg/m³
A	Swept area of the wind turbine rotor	m²
π	Pi (constant, approximately equal to 3.14159)	rad
r	Rotor radius of a wind turbine	m
t	Time	sec
P_{wind}	Amount of wind power that could be available	Watts (W)
P_{Turbine}	Mechanical power of the wind turbine	Watts (W)
C_{p}	Power coefficient of the wind turbine	Unitless
λ	Wind turbine tip speed ratio	Unitless
V_{m}	Wind turbine generator's angular speed	rad/s
β	Blade angle	rad
$c_1, c_2, c_3, c_4, c_5, c_6$	Coefficients depending on the type of wind turbine	Various (as per specific model)
λ_i	Adjusted tip speed ratio	Unitless
ω_m	Angular velocity of the wind	rad/s

 DOI: 10.22266/ijies2025.0731.28

Received: April 13, 2025. Revised: May 20, 2025.

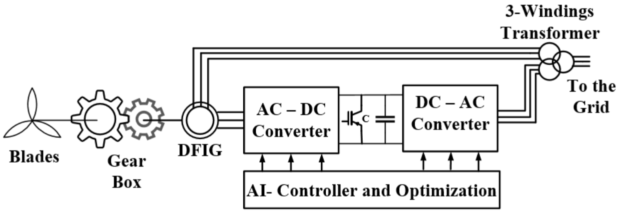

Figure. 2 Proposed system configuration

3.2 Proposed system

The research utilizes MATLAB/Simulink software and real-time hardware systems to construct a DFIG-Wind turbine system model integrated with an electrical network using a constant voltage by frequency model. The model is interfaced through the Lucas-Nülle machine and power electronics laboratory equipment. DFIG control performance is demonstrated using eigenvalue analysis with time-domain simulation on a single sample DFIG of the Infinite Machine Bus (SMIB) system.

DFIG is a typical wind turbine producer featuring a stator previously connected to the power grid; a converter links the rotor to the grid. A converter typically comprises a rotor-side-controlled (RSC) converter and a grid-side-controlled (GSC) converter. The RSC regulates the rotor current, which controls the active and reactive power flow of a DFIG. Meanwhile, the controlled GSC maintains a constant DC link voltage and prevents reactive power exchange in the stator through the grid. Table 3 describes the specifications of the turbine used in this experiment.

3.3 Wind turbine model with DFIG

DFIG dynamics by wind turbines and stability in controlling design may all be investigated using an SMIB system. Through control systems, wind turbines, drive trains, induction generators, and back-to-back PWM converters are interconnected with infinite bus transformers. The DFIG wind turbine control system operates with two distinct management layers: wind turbine and DFIG management. Using DFIG control

Table 3. Wind Turbine Specifications

Parameter	Value	Unit
Rated Power	0.8	kWatt
Rated Voltage	208/120	Volt
Rated Speed	1400/1500/1600	RPM
Rated Current	3.5 (DC) / 2 (AC)	Amp.
Excitation Voltage	24 (DC) / 130 (AC)	Volt
Excitation Current	4 (AC) / 11 (DC)	Amp.
Power Factor (cos ϕ)	0.75	
Max. Speed	4000	RPM
Max. Torque	30	N.m
Rotor Diameter	90	m
Type of Generator	Doubly Fed Induction Generator	

Using the wind turbine's reference rotor speed and pitch angle as a reference, a wind turbine level control determines the reference rotor speed and pitch angle. The power optimization approach utilizes an underrated turbine speed, whereas the power limiting strategy employs an overrated one. [18, 19]. The level control of DFIG encompasses both rotor and grid control enabling the management of active and reactive power by controlling the DFIG through the switch vector.

3.4 Hybrid control strategy

To enhance the performance of the DFIG-based wind energy system under varying wind and load conditions, a hybrid control strategy is proposed, combining a PSO-tuned PI controller, a Fuzzy Logic Controller (FLC), and an Adaptive Neuro-Fuzzy Inference System (ANFIS). Supervisory control logic governs the interaction between these controllers, ensuring optimal selection based on real-time system dynamics. The hybrid system operates in a parallel structure, with a supervisory decision layer evaluating system states, such as error magnitude, rate of change of error, and wind speed fluctuations, to determine which controller output to apply. The control actions are defined as follows:

i. PI-PSO Controller: This controller is active under normal operating conditions with moderate wind variation; it ensures stability and basic control accuracy.
ii. FLC: Triggered when the system experiences nonlinear transient behavior or rapid variations in wind input.
iii. ANFIS: Engaged when the system operates under uncertain or highly dynamic conditions, requiring adaptive learning and response.

As illustrated in Fig. 3, the supervisory unit uses a rule-based switching mechanism to select the appropriate control signal. Mathematically, the final control output $U(t)$ applied to the RSC (Rotor Side Converter) is defined as:

$$U(t) = \begin{Bmatrix} U_{PI-PSO}(t), & if\ |\Delta e(t)| < \varepsilon \\ U_{FLC}(t), & if\ \varepsilon_1 \leq |\Delta e(t)| < \varepsilon \\ U_{ANFIS}(t), & if\ |\Delta e(t)| \geq \varepsilon \end{Bmatrix}$$

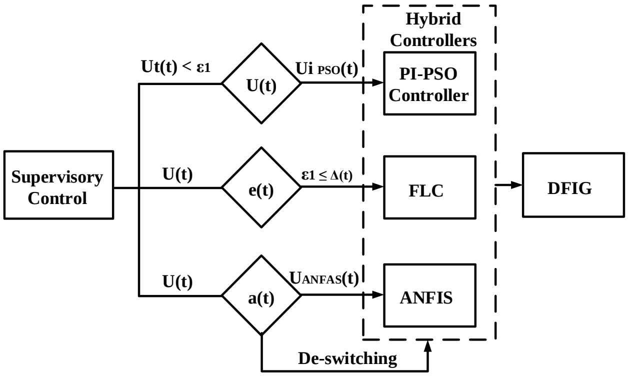

Figure. 3 A Hybrid Control Strategy of the DFIG

where $\Delta e(t)$ is the error variation rate, and ε_1, ε are predefined thresholds for switching logic.

4. Mathematical model

4.1 DFIG model

The DFIG is an equivalent voltage source utilizing the transient impedance circuit for power system stability analysis. [1, 20]. The induction generator differential equations related to the internal basic circuit, the stator current, and the equivalent voltage behindhand transient impedance is expressed in the (d-q) frame of reference rotating at synchronous speed, considering the states of the variables.

Therefore, the fourth-order model of the generator, as described in Eqs. (1)-(4) [21] is required for this work control design.

$$\frac{1}{\omega_b}\frac{di_{ds}}{dt} = -\frac{\omega_s}{X_s'}\left(R_s + \frac{X_s - X_s'}{\omega_s T_0}\right) i_{ds} + \omega_s i_{qs} + \frac{\omega_r}{X_s'} e_{ds}' - \frac{1}{X_s' T_0} e_{qs}' + \frac{\omega_s L_m}{X_s' L_r} u_{dr} - \frac{\omega_s}{X_s'} u_{ds} \quad (1)$$

$$\frac{1}{\omega_b}\frac{di_{qs}}{dt} = -\omega_s i_{ds} - \frac{\omega_s}{X_s'}\left(R_s + \frac{X_s - X_s'}{\omega_s T_0}\right) i_{qs} + \frac{1}{X_s' T_0} e_{ds}' + \frac{\omega_r}{X_s'} e_{qs}' + \frac{\omega_s L_m}{X_s' L_r} u_{qr} - \frac{\omega_s}{X_s'} u_{qs} \quad (2)$$

$$\frac{1}{\omega_b}\frac{de_{ds}'}{dt} = -\frac{1}{T_0}\left[e_{ds}' - (X_s - X_s') i_{qs}\right] + (\omega_s - \omega_r) e_{qs}' - \frac{\omega_s L_m}{X_s' L_r} u_{qr} \quad (3)$$

$$\frac{1}{\omega_b}\frac{de_{qs}'}{dt} = -\frac{1}{T_0}\left[e_{qs}' + (X_s - X_s') i_{ds}\right] - (\omega_s - \omega_r) e_{ds}' + \frac{\omega_s L_m}{L_r} u_{dr} \quad (4)$$

where "$i_s = i_{ds} + j i_{qs}$ a stator of the current path; $e's = e'ds + je'qs$ and a path of equivalent voltages behind the transient impedance is essential $e_{ds}' = -\frac{\omega_s L_m \psi_{qr}}{Lr}, e_{qs}' = \frac{\omega_s L_m \psi_{dr}}{L_r}$; $u_s = u_{ds} + j u_{qs}$ is the stator voltage vector; $u_r = u_{dr} + j u_{qr}$ is the rotor voltage vector; $L_s = L_m + L_{ls}, L_r = L_m + L_{lr}, X_s = \frac{\omega s}{Ls}$, $X_s' = \omega_s\left(L_s - \frac{L_m^2}{Lr}\right), T_0 = \frac{L_r}{R_r}$. In this model, the generation of stator and rotor currents flows positively and negatively. [22].

4.2 Wind turbine in drive train model

The best analysis of wind stability using a two-mass model of a traction drive, since a wind turbine shaft is more flexible than a conventional power plant [23]. The following are the equations for the train driver's two-mass model.

$$\frac{d\omega_r}{dt} = (T_{sh} - T_e - B\omega_r)\ \frac{1}{2H_g} \quad (5)$$

$$\frac{d\theta_t}{dt} = (\omega_t - \omega_r)\omega_b \quad (6)$$

$$\frac{d\omega_t}{dt} = \frac{1}{2.0H_t}(T_m - T_{sh}) \quad (7)$$

where H_g and H_t Are the inertia constants of the generators and turbines, respectively. The electromagnetic torque supplies wind turbine power T_e .The shaft torque supplied to the wind turbine is T_{sh} and mechanical torque T_m.

$$T_e = (i_{dr}.i_{qs} - i_{qr}.i_{ds})\ L_m \quad (8)$$

$$T_{sh} = K_{sh}.\theta_t + D_{sh}.\omega_b.(\omega_t - \omega_r) \quad (9)$$

$$T_m = \frac{\rho\pi C_p(\lambda,\beta)V_w^3}{2\times\omega_t} \quad (10)$$

The power coefficient C_p is

$$C_p = \frac{50}{11}\left(\frac{116}{\lambda_i} - \frac{\beta}{2.5} - 5\right) e^{-12.5\times\lambda_i} \quad (11)$$

$$\lambda_i = \frac{1}{\frac{1}{(\lambda + 0.08\,\beta)} - \frac{200}{7\times(\beta^3+1)}} \quad (12)$$

The power-speed characteristic curve sets the generator speed reference. [24]. To represent the rotor speed reference along this curve, we may use the formula for generator speed as

$$\omega_{ref} = \sqrt{\frac{T_m}{K_{opt}}} \quad (13)$$

Received: April 13, 2025. Revised: May 20, 2025.

The operation is based on DFIG and is driven by the speed, torque, and power values needed to maintain the turbine wind system. The pitch angle should be zero when the turbine speed tops $12\ m/s$, that wind speed was tested at the rated power of a $2\ MW$ turbine. When the turbine speed exceeds the permitted winding speed, the pitch angle must be adjusted to control the DFIG's rotation at a rated speed, torque, and power. Adjusting blade pitch angles is necessary to reduce turbine output in high winds. The pitch servo concept.

$$\frac{d\beta}{dt} = \frac{1}{T_\beta}(\beta_{ref} - \beta) \tag{14}$$

4.3 Rotor Siding of Converter

The rotor siding of the converter's generally controlling architecture is shown. When the stator flux is oriented in the appropriate path, it may be said that the stator flux is $\psi_{ds}^{\varphi} = \psi_s \ and\ \psi_{ds}^{\varphi} = 0$.

$$u_{dr}^{\phi} = -(\omega_s - \omega_r)\sigma L_r i_{qr}^{\phi} + K_{Pir}\left(I_{dref} - i_{dr}^{\phi}\right) + x_{idr} \tag{15}$$

$$u_{qr}^{\phi} = (\omega_s - \omega_r)\left(\sigma L_r i_{dr}^{\phi} + \frac{L_m \psi_s}{L_s}\right) + K_{Pir}\left(i_{qrref}^{\varphi} - i_{qr}^{\phi}\right) + x_{\dot{\imath}qr} \tag{16}$$

where $\sigma = 1 - \frac{L_m^2}{L_s L_r}$ is a leakage factory.

A rotor-side converter's control equation is,

$$\dot{x_\omega} = \frac{K_{P\omega}}{T_{I\omega}}(\omega_{ref} - \omega_r) \tag{17}$$

$$x_{\dot{\imath}dr} = \frac{K_{Pir}}{T_{Iir}}\left(I_{dref} - i_{dr}^{\phi}\right) \tag{18}$$

$$i_{qrref}^{\phi} = \frac{L_s}{L_m \psi_s}[K_{P\omega}(\omega_{ref} - \omega_r) + \chi_\omega] \tag{19}$$

$$x_{\dot{\imath}qr} = \frac{K_{Pir}}{T_{Iir}}\left(i_{qrref}^{\varphi} - i_{qr}^{\phi}\right) \tag{20}$$

where K_P and T_I are the rotor speed control loop's related gain and integral time constant, respectively. Similarly, K_{Pir} and T_{Iir} are parameters that influence the rotor current's relative gain by controlling the loop. It determines the essential time constant. We suppose that the rotor current control loop's d and q-component parameters are identical to simplify the analysis. The relation between generating with the reference surround and the reference stator-flux-oriented controlling:

$$\begin{bmatrix} y_{dr} \\ y_{qr} \end{bmatrix} = \begin{bmatrix} \cos\varphi & -\sin\varphi \\ \sin\varphi & \cos\varphi \end{bmatrix} \begin{bmatrix} y_{dr}^{\varphi} \\ y_{qr}^{\varphi} \end{bmatrix} \tag{21}$$

where y is represented by a current or voltage, and the angle $\varphi = \arctan\left(\frac{\psi_{qs}}{\psi_{ds}}\right)$ represents the angle among the stator's flux vector in the d-axis in a generating mode, which is the position of the rotor relative to the stator reference frame [22].

4.4 Grid side converter

DFIG-based WECS maintains a constant voltage through the DC link and manages the activation of reactive power output to meet grid requirements. The GSC of the DFIG is often controlled via a voltage within a capacitor (VC). This strategy breaks down the GSC currents into active and reactive power components. The dynamic on reactive powers of a GSC can now be independently controlled; make sure the GSC's differential equations are provided by

$$\frac{di_{Dl}}{dt} = \frac{\omega_b}{L}\left(u_{ds} - R_L i_{Dl} + \omega_s L i_{Ql} - u_{da}\right) \tag{22}$$

$$\frac{di_{Ql}}{dt} = \frac{\omega_b}{L}\left(u_{qs} - R_L i_{Ql} - \omega_s L i_{Dl} - u_{q\,a}\right) \tag{23}$$

as $i_L = i_{Dl} + j\, i_{Ql}$ is a grid-siding of the inductor current rectifier and $u_a = u_{da} + j\, u_{qa}$ is a GSC voltage regulator [25]. Based on this reference frame, we may deduce that u = U, and the grid voltage always equals zero. The grid-side converter voltage equations may be constructed using the control technique equation:

$$U_{da}^{\varepsilon} = U_s + \omega_s L i_{Ql} - \left[K_{PiL}\left(i_{dLref}^{\phi} - i_{Dl}^{\phi}\right) + \chi_{idL}\right] \tag{24}$$

$$u_{qa}^{\phi} = -\omega_s L i_{Ql} - \left[K_{PiL}\left(I_{qlref} - i_{Ql}^{\phi}\right) + x_{\dot{\imath}qL}\right] \tag{25}$$

The following are equations for the grid-siding of the converter controller:

$$\dot{x_v} = \frac{K_{Pv}}{T_{Iv}}(U_{ref} - U_{dc}) \tag{26}$$

$$i_{qLref}^{\phi} = \frac{\sqrt{2}}{\sqrt{3}\,m}[K_{Pv}(U_{dcref} - U_{dc}) + \chi_v] \tag{27}$$

$$\dot{x_{1dL}} = \frac{K_{PiL}}{T_{IiL}}\left(I_{dLref} - i_{Dl}^{\phi}\right) \tag{28}$$

$$\dot{x_{1qL}} = \frac{K_{Pir}}{T_{Iir}}\left(i_{qLref}^{\varphi} - i_{Ql}^{\phi}\right) \tag{29}$$

The DC link controls the voltage loop's relative gain K_{Pv} usually, the integral time constant T_{Iv} are given. A grid-siding of the inductor current controlling the loop's proportional gain and essential time steady are K_{PiL} and T_{Iir}. The grid-side inductor current control loop's d- and q-component parameters are also expected to be the same. The generating reference frame relates to the grid-voltage-oriented framing with the reference given by the equation

$$\begin{bmatrix} Y_{da} \\ y_{qa} \end{bmatrix} = \begin{bmatrix} \cos\varepsilon & -\sin\varepsilon \\ \sin\varepsilon & \cos\varepsilon \end{bmatrix} \begin{bmatrix} y_{da}^{\varepsilon} \\ y_{qa}^{\varepsilon} \end{bmatrix} \tag{30}$$

where "$\varepsilon = \arctan\left(\frac{u_{qs}}{u_{ds}}\right)$ is the angle between the grid's voltage vector in the generator reference frame and the d-axis represents the grid's phase alignment with the generator's rotating reference frame. This angle is crucial for synchronizing the generator with the grid and is vital in vector control strategies for DFIG-based wind power systems.

4.5 DC-link capacitor

The calculation may describe the DC-link capacitor's energy balance:

$$\frac{C_{dc}U_{dc}}{\omega_b}\frac{dU_{dc}}{dt} = P_a - P_r = \frac{3}{2}\left(u_{da}i_{Dl} + u_{qa}i_{Ql} - u_{dr}i_{dr} - u_{qr}i_{qr}\right) \tag{31}$$

P_a and P_r are the grid-sides of the converters and rotor circuit power, respectively, are provided by the DC-link voltage U_{dc} [26]. In this work, the endless bus is a model for interaction between the internal system and the outside world.

$$U_s\angle\theta_s - E_0\angle 0 = (Z_T + Z_L)(i_s - i_L) \tag{32}$$

4.6 Wind turbines model

The obtainable energy in the wind determines the efficiency of converting it into turbine energy for changing systems. The moving energy of many air particles has a total mass of m and moves at the wind speed. It is possible to treat it as a form of wind energy. The model can explain the potential kinetic energy stored in the wind if all air molecules are moving in the same direction and at the same speed before hitting the rotor blades of a wind farm. [26, 27]. The kinetic energy of moving air particles

$$E = \frac{1}{2}mV_w^2 \tag{33}$$

where m are the air particles of the whole mass, V_w are the air atoms' velocities. Because the air molecules are moving at the same speed, the total mass over time t materials can be rewritten in many modules in the following ways:

$$m = \rho A V_m t = \rho\pi r^2 V_w t \tag{34}$$

A represents the swept area. A of the rotor's turbine, and ρ represents air density. a radius r of the swept part by the wind blades. The kinetic energy of air units can be expressed as:

$$E = \frac{1}{2}\rho\pi r^2 V_w^3 t \tag{35}$$

The power of winning can be seen at any given time, as follows.

$$P_{wind} = \frac{E}{t} = \frac{1}{2}\rho\pi r^2 V_w^3 \tag{36}$$

where P_{wind} is the amount of wind power that could be available. The relationship between power taken by the turbine and the wind's extreme potential power is as follows:

$$C_p = \frac{P_{Turbine}}{P_{Wind}} \tag{37}$$

where $P_{Turbine}$ represents a mechanical rule generated by the turbine, C_p its the control coefficient of a turbine, and P_{wind} is Power wind, which, as expressed in the following [28].

$$C_p = c_1 \times \left(\frac{c_2}{\lambda_i} - c_3.\beta - c_4.\beta^x - c_5\right)e^{-\frac{c_6}{\lambda_i}} \tag{38}$$

where,

$$\frac{1}{\lambda_i} = \frac{1}{\lambda + 0.08\beta} - \frac{7}{200\times(1.0+\beta^3)} \tag{39}$$

where λ represents the tip speed ratio of wind turbines and is given by $\lambda = \frac{w_m r}{V_m}$, β is the angle blade and V_m is the wind generator's angular speed. The coefficients ($c_1 \sim c_6$) have dissimilar values depending on the wind turbine. As a result, the wind turbines' power can be rewritten as follows:

Received: April 13, 2025. Revised: May 20, 2025.

$$P_{Turbine} = \frac{1}{2}\rho.\pi.r^2.C_p(\lambda,\beta).V_W^3 \quad (40)$$

A DFIG-based wind energy conversion system (WECS) gearbox is necessary to match the wind turbine rotor's low-speed rotation with the generator's high-speed rotation. It effectively increases the rotational speed of the mechanical energy input, ensuring that the generator operates optimally to convert mechanical energy into electrical energy. The AC/DC/AC converter connected to the gearbox contains an RSC and GSC associated with the back-to-back through a DC link. This setup enables precise control of the rotor currents, which is essential for optimizing DFIG's power output and maintaining a stable grid connection. The final stage involves connecting the generated electrical energy to the grid's power. The stator of the DFIG is directly connected to the grid, ensuring continuous energy transfer. Meanwhile, the rotor interacts with the grid through the AC/DC/AC converter, enabling bidirectional power flow and enhanced system control.

4.7 Operational modes of DFIG

DFIG is the system's core component, specifically designed to convert the mechanical energy from a turbine into electrical energy. As previously mentioned, its unique feature is its capability to operate at sub- and super-synchronous speeds, enabling more efficient and flexible energy generation.

DFIG can operate in binary distinct styles, sub-synchronous and super-synchronous, based on the rotor's speed relative to the grid's synchronous speed. In this mode, DFIG absorbs power from the grid, effectively behaving like a motor. This model is beneficial in low wind conditions, where the generator needs additional power. In this mode, DFIG operates as a variable-speed wind generator, allowing it to continue generating power even when wind speeds are lower than ideal.

5. Simulink model of proposed system

Wind turbine model: This block simulates the mechanical input to the DFIG, typically based on wind speed profiles.

DFIG Model: This is the system's core. The DFIG connects the rotor to the grid through a buck converter. This block includes models of the stator, rotor, and the magnetic coupling between them. Figs. 5 to 7 show the proposed system configuration using MATLAB/Simulink. The converters' rotor and grid sides utilize power electronics and are connected to the rotor and grid, respectively. Electronics control the rotor current, thereby converting active and reactive power between the rotor and the grid. They usually use vector control techniques to control usage. This is another power electronic conversion associated with the generator in a rotor connecting to a grid.

5.1 Particle swarm optimization (PSO)

In DFIG-based turbine systems, PI controllers are widely used in the control loops of the RSC and GSC converters. They sufficiently tuned PI controller parameters (the proportional and integral gains $in\ are\ K_p$ and K_i respectively), which are essential for efficient, stable action of the DFIG structure, the velocity V_{i+1} of the particle i using the equation:

$$V_{i+1} = w.V_i + c_1.rand(\quad).\left(P_{best,i} - X_i\right) + c_2 .rand(\quad).(G_{best} - X_i) \quad (41)$$

For each particle i , where $(i = 1, 2, \ldots, N)$, randomly initialize its position X_i within the feasible range of K_p and K_i Values and initialize its velocity V_i to a small value [29].

The particle's best-known position $P_{best,i}$ to its initial position X_i, and set the global best-known position G_{best} to the $P_{best,i}$ of the particle with a good value in the objective function rating.

Then, update the position of a particle i using the equation:

$$X_{i+1} = X_i + V_{i+1} \quad (42)$$

After a predetermined number of iterations, or if G_{best} stops improving significantly, the algorithm is considered to have converged. The final G_{best} contains the PI controllers' optimal K_p and K_i values.

Utilize the K_p and K_i values obtained from the final G_{best} to configure the PI controller parameters in the RSC–GSC of the DFIG system.

5.2 Cost function

The PSO algorithm optimizes the PI controller parameters. (K_p, K_i) based on the performance index defined by the Integral of Time-weighted Absolute Error (ITAE):

$$J = \int_0^t t.|e(t)|dt$$

where e(t) is the error between the reference value and the actual output, this cost function was selected

Table 4. The PSO algorithm parameters

Parameter	**Value**
Swarm Size	30 particles
Maximum Iterations	100
Inertia Weight (w)	Linearly decreasing from 0.9 to 0.4
Cognitive Coefficient (c1)	2
Social Coefficient (c2)	2
Velocity Limits	$[-V_{max}, V_{max}]$ based on each parameter range
Parameter Bounds	$Kp \in [0, 10], Ki \in [0, 5]$
Stopping Criteria	Maximum iterations or convergence tolerance $\varepsilon < 0.001$

to minimize overshoot, settling time, and steady-state error.

The PSO algorithm was configured using the following parameters:

A convergence plot was generated to visualize the optimization process. It shows the decrease in the cost function (ITAE) across iterations, confirming the effectiveness and stability of the PSO strategy.

5.3 Speed control by fuzzy and ANFIS controllers

In a DFIG-based turbine system, controlling the generator speed is crucial for maximizing power extraction from the wind and ensuring stability. Fuzzy logic control (FLC) and Adaptive Neuro-Fuzzy Inference System (ANFIS) are techniques used to control the speed of DFIG, with mechanical torque being the primary control action.

5.3.1. Inputs to the controller

In this scenario, the primary input for fuzzy control is the speed error, which is defined as the difference between the desired and actual speeds of the DFIG. A second input is the rate of alteration of this speed error (i.e., how quickly the speed error changes), which can be considered equivalent to the derivative in a PID controller.

5.3.2. Fuzzy sets and membership functions

Fig. 4 shows the membership used in the current work using the Fuzzy and ANFIS controllers.

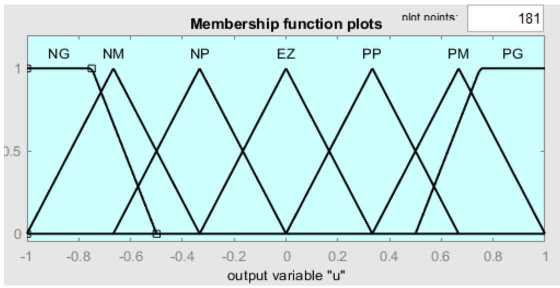

(a)

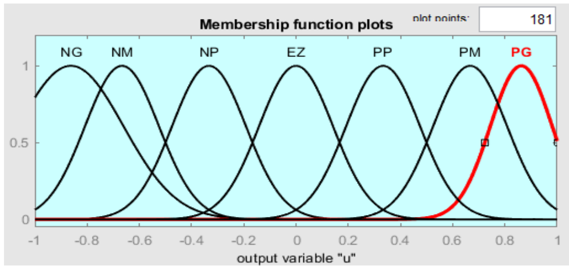

(b)

Figure. 4 Membership is used in the current work: (a) Fuzzy membership and (b)ANFIS membership function

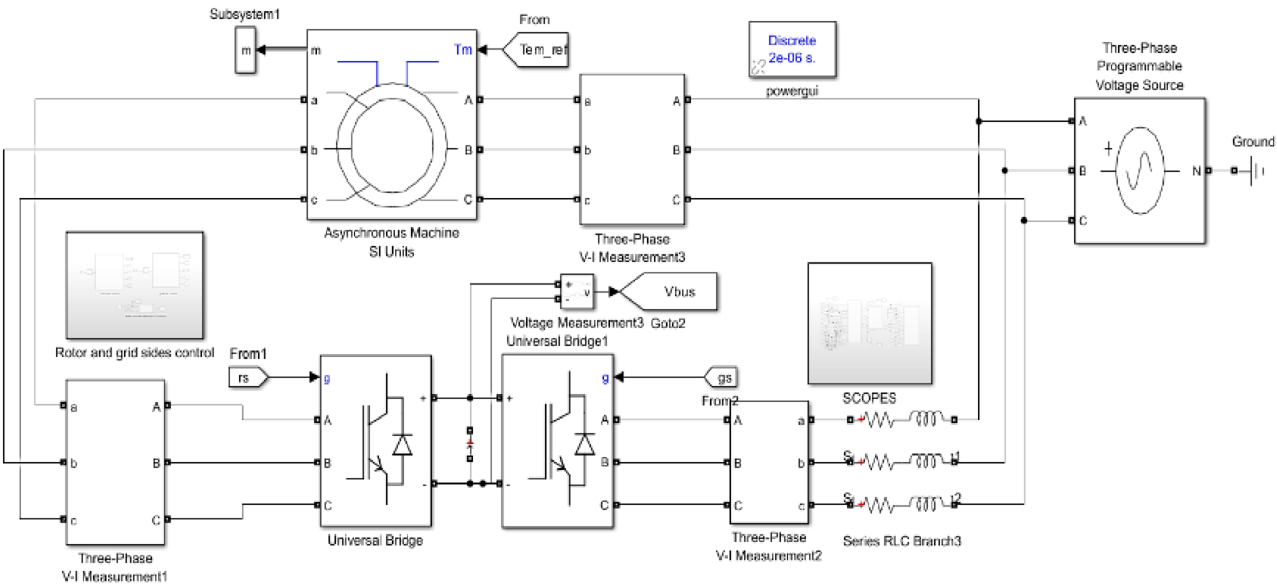

Figure. 5 The proposed model of the DFIG utilizes a control strategy developed in MATLAB/Simulink

Received: April 13, 2025. Revised: May 20, 2025.

Various fuzzy linguistic variables used to represent different magnitudes of input or output values in a fuzzy logic control system might include "PS (Positive - Small)," "PB, (Positive Big)," "NS (Negative Small)," "NB (Negative Big)," and "ZE (Zero)", though the exact terms can vary. Each rule defines a relationship between the inputs and a result that uses an output action. For example, a rule might be: "If the speed error is PS and a change of fault is NS, after this process, the torque is Positive Medium (PM)."

Inference and Aggregation: Based on the current inputs (speed error and its rate of change), the fuzzy controller evaluates all 49 rules. This is the inference process:

Defuzzification: The aggregated fuzzy output set is converted into a single, crisp (non-fuzzy) value. This is the mechanical torque value that will be applied to DFIG. The DFIG responds to this torque input by adjusting its speed. This, in turn, changes the speed error, and the cycle repeats.

One of the strengths of using fuzzy and ANFIS controllers in this context is their ability to handle nonlinearities and uncertainties in the DFIG system. They are based on rules that can be easily understood and modified, allowing for intuitive design and tuning. Fuzzy logic control and ANFIS are advanced methods for controlling speed in a DFIG, with mechanical torque being the primary control action. [30]. Table 5 describes the parameters of DFIG used in this work. Fig. 9 illustrates the hardware components utilized in this work and their interfaces with the control methods.

Table 5. Specification parameters of DFIG

Parameters	**Value**	**Unit**
Stator resistor R_s	0.0026	Ω
Rotor resistor R_r	0.0029	Ω
Stator inductor L_s	2.586	mH
Rotor inductor L_r	2.586	mH
Magnetizing inductance L_m	2.5	mH
Moment of inertia J	135	$kg \cdot m^2$
Damping factor D	0.8×10^{-3}	N·m/rad/s
Frequency	60	Hz
DC Link capacitor	0.018	F

5.3.3. ReaL-time setup with Lucas-Nülle platform

To validate the proposed hybrid control strategy's real-time applicability, a hardware-in-the-loop (HIL) test was conducted using the Lucas-Nülle (LN) platform integrated with MATLAB/Simulink. The Simulink model runs in external mode and interfaces with the LN hardware via a TCP/IP communication protocol over RS-232. The real-time control loop operates with a fixed sampling rate of 1 millisecond (1 ms), ensuring synchronized execution with the physical system. All control commands and feedback signals are exchanged in real time. Table 6 shows the system configuration parameters Fig. 6 shows a proposed MATLAB/Simulink interface using an LN system in the Power/Machine lab. Fig. 7 shows the MATLAB interface simulation with an LN system in the Power/Machine lab using an ANFIS controller.

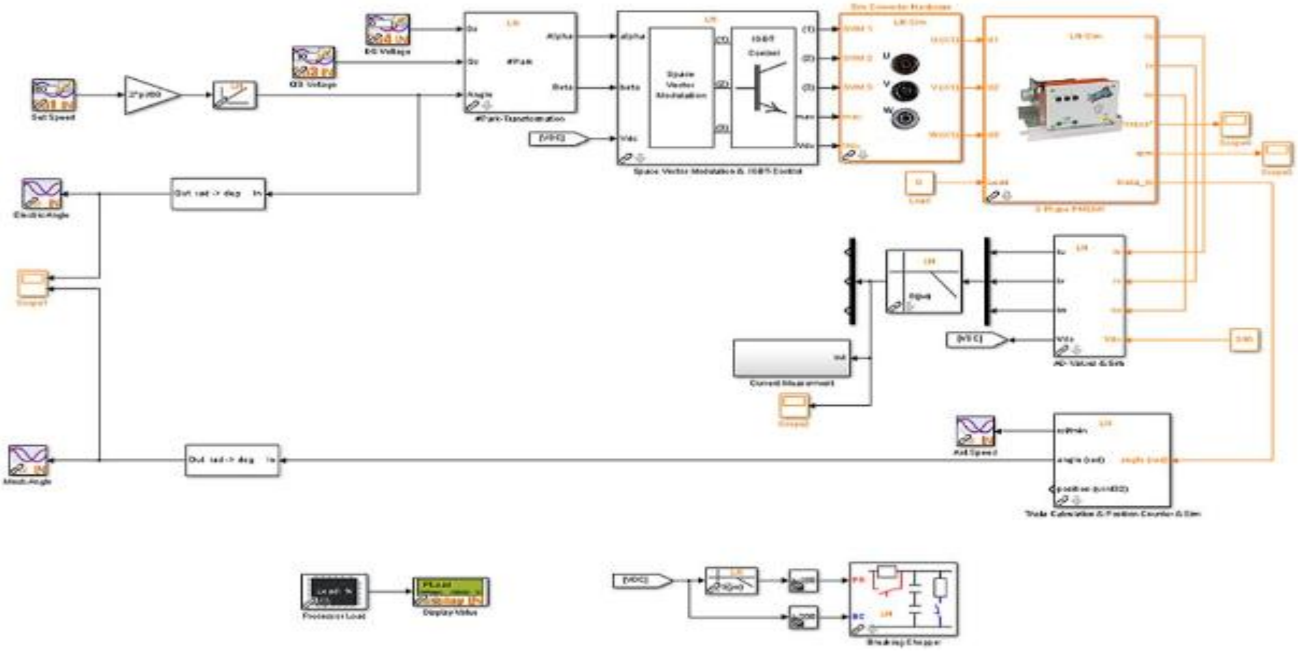

Figure. 6 A proposed MATLAB/Simulink interface using an LN system in the Power/Machine lab

Received: April 13, 2025. Revised: May 20, 2025.

Table 6. System Configuration Parameters

Parameter	Value
Control Loop Execution Time	1 ms
Communication Protocol	TCP/IP
Interface Type	RS-232 Serial
Simulation Environment	MATLAB/Simulink (External Mode)
LN System Mode	Real-Time Execution
Platform Role	Wind Emulator and Grid Interface
Data Exchange Frequency	1 kHz (synchronized with sampling time)

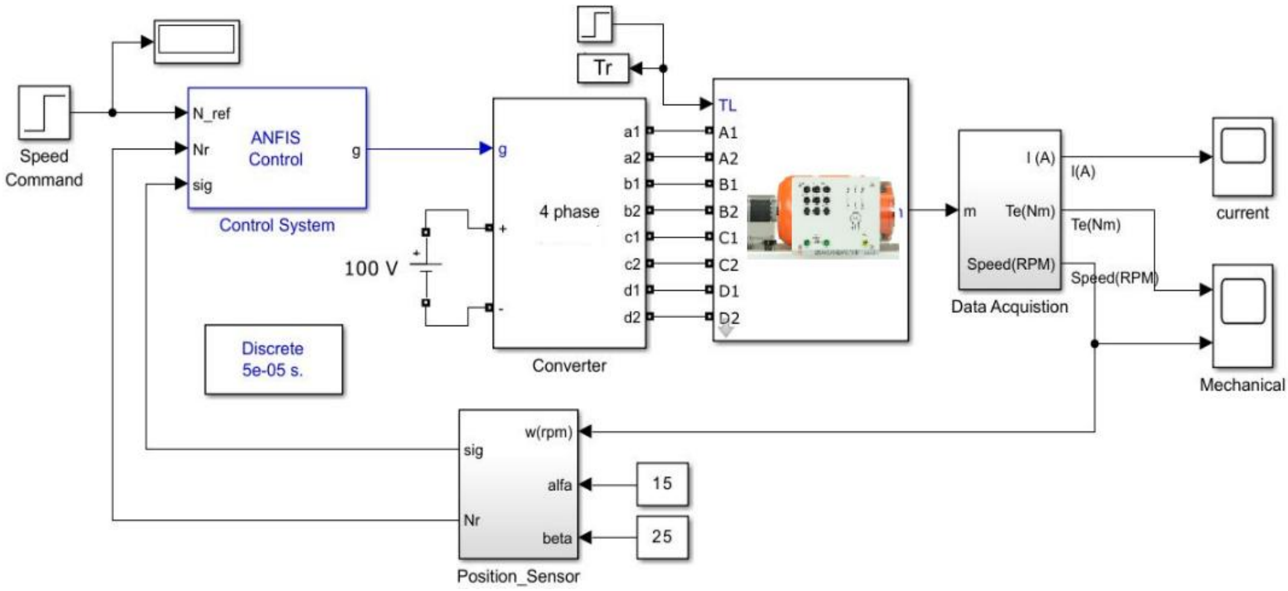

Figure. 7 The MATLAB interface simulation with an LN system in the Power/Machine lab using an ANFIS controller

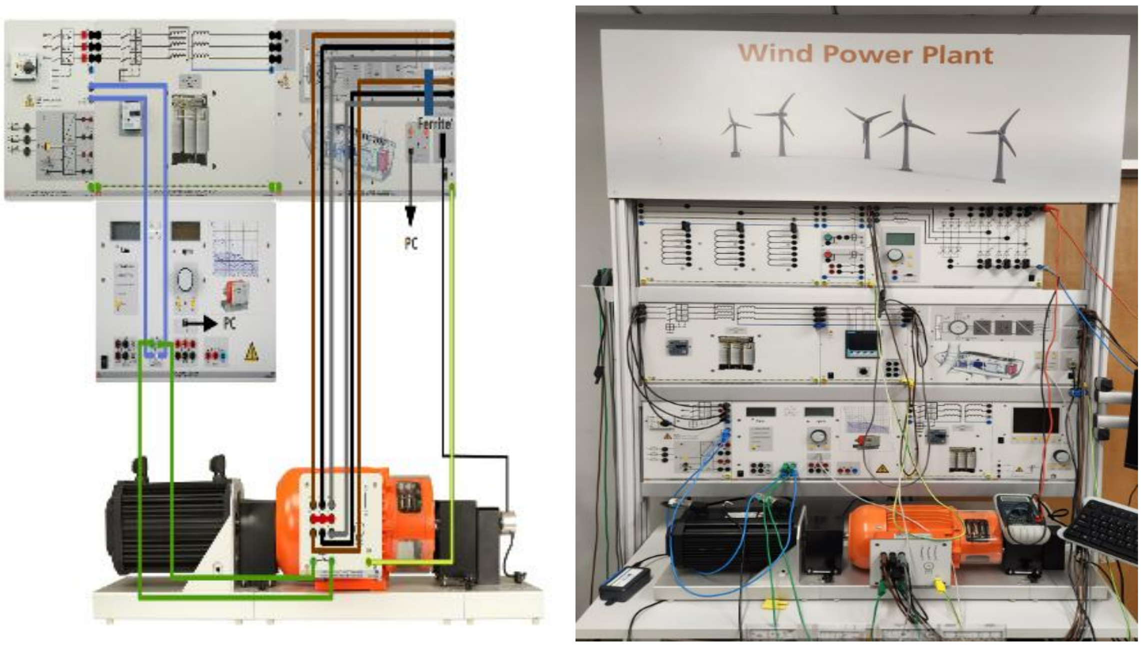

(a) (b)

Figure. 8 The wiring diagram of the wind turbine system: (a) Wiring connection and (b) Hardware implementation

Received: April 13, 2025. Revised: May 20, 2025.

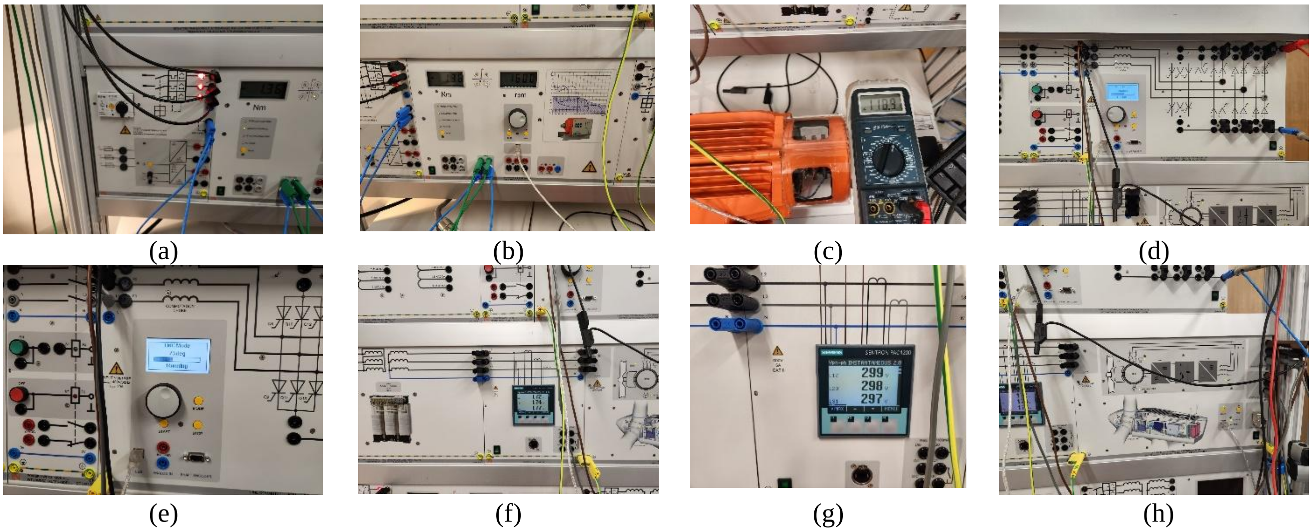

Figure. 9 The hardware components: (a) SMIB system, (b) Servo machine, (c) DFIG with meter, (d) Rectifier circuit, (e) Delay angle regulator, (f) Transformer model, (g) Measurement meter, and (h) DFIG model

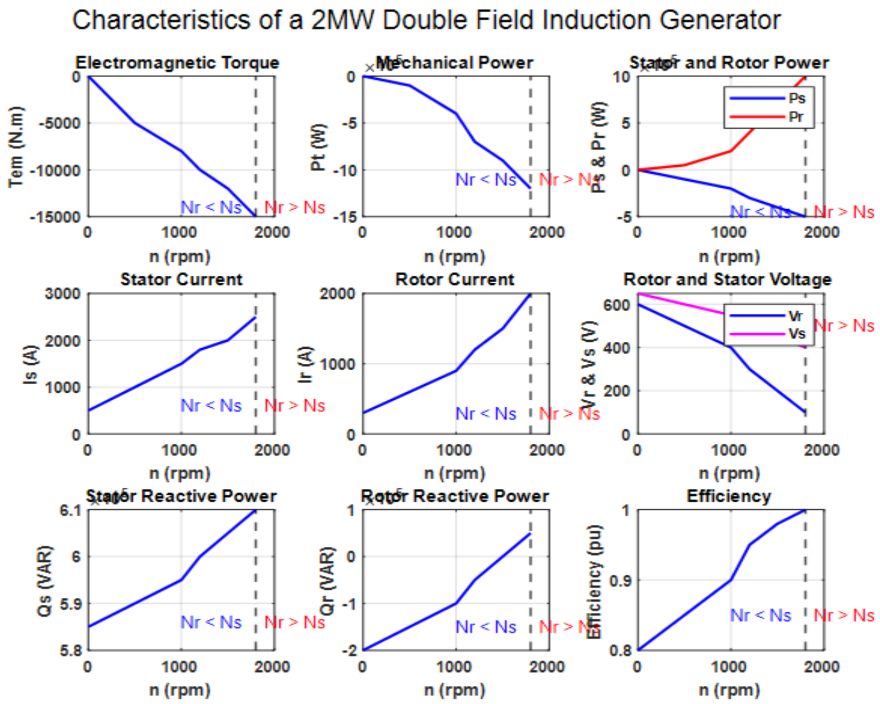

Figure. 10 Steady-state characteristics of a 2MW DFIG $I_{dr} = 0$, under two operational modes

Fig. 9 shows Hardware components, including SMIB system, Servo machine, DFIG with meter, Rectifier circuit, Delay angle regulator, Transformer model, Measurement meter, and DFIG model.

6. Results and discussion

This section examines the advanced control strategies utilized in real-time DFIG systems for wind energy conversion, focusing on three primary controllers: PSO-PI controllers, PSO-FLC, and PSO-ANFIS. These controllers play a crucial role in optimizing the operation of DFIG schemes, ensuring resilience against external disturbances such as variable turbine speeds and grid disturbances while maintaining the quality of power fed into the grid.

6.1 Design DFIG under steady-state analysis

A DFIG connects the stator and rotor to the grid. In contrast, the rotor is directly associated with the stator in back-to-back converters, allowing the power to depend on the active and reactive power switches. DFIG is typically used in turbines due to its flexibility in control, ability to operate efficiently, and wide range of speeds. Fig. 10 shows a steady state analysis,

Received: April 13, 2025. Revised: May 20, 2025.

which discusses the behavior of results in two modes: sub-synchronous mode and super-synchronous mode [31, 32].

Sub-Synchronous Mode: rotor speed, N_r is lower than the synchronous speed N_s (1800 RPM). Once the wind speed is below the rated speed, this is a usual mode of operation, and the DFIG operates like a motor drawing reactive power from the grid.

Super-Synchronous Mode*:* rotor speed, N_r is higher than the synchronous speed N_s occurs when the turbine speed exceeds the rated speed.

The power flow direction through the rotor side on the converter is reversed. Instead of consuming power from the grid (as in sub-synchronous mode), it routes the extra power produced in the rotor circuit back to the grid. Fig. 10 shows the steady-state characteristics of $2\,MW$ DFIG, $I_{dr} = 0$ under two operational modes. The electrotechnical torque decreases with increasing rotational speed because of the range $N_r < N_s$. The generator is operating as a generation system. At the same time, when $N_r > N_s$, it contributes to the power injection into the grid. Additionally, mechanical power is converted to electric power at speeds exceeding the synchronous speed N_s limit. At the same time, it is harmful at low speeds, where the generator needs additional support to operate. The transferring of power between the rotor and the stator. When $N_r < N_s$, the power is absorbed from the grid, and when $N_r > N_s$, the power is injected into it. The stator current increases with increasing speed, indicating that the electrical power requirement of the generator increases as the speed increases. Additionally, the rotor current increases with cumulative speed up to synchronous speed and then decreases after exceeding it, due to the rotor's reduced current requirement within the synchronous range. The stator voltage increases with increasing rotor speed, while the rotor voltage increases at higher speeds, reflecting the generator's operation under these conditions. The reactive power in the stator, aside from rotor consumption or injection of reactive power, varies with the rotor's speed, affecting the grid's stability. Efficiency improves as speed increases to synchronous speed, then declines at very high speeds due to losses in electrical and mechanical components.

6.2 DFIG based on PI-PSO controller

This simulation model determines the system's outputs according to the equations related to the voltage inputs and the machine's characteristics. The steady-state points of the machine, analyzed in the preceding sections, depend on the applied voltages and the load torque. A 2MW DFIG specification is listed in Table1 . The hardware equipment was developed using AI techniques from the LN machine and the Power Electronics Lab, and a closed-loop control system project using MATLAB and Simulink.

The analysis of simulation results depends on the variable speed of the turbine when investigating the reactive power, which is the aim of the design presented in this paper. Fig. 11a illustrates the wide range of varying turbine speeds, from 5 m/s at 4 s to 11 m/s, applied to validate the DFIG with the wind turbine (WT) system. Meanwhile, Fig. 11b illustrates the evolution of DFIG speed. It can be observed from this figure that an MPPT regulator can better manage the rotational speed of a generator to extract the maximum power from it, depending on the applied wind speed. The dynamic response of the rotor speed tracks the wind. The d-axis's dynamic response is to maintain zero during variable wind speed. The power output generated by a DFIG is illustrated in Fig. 11c.

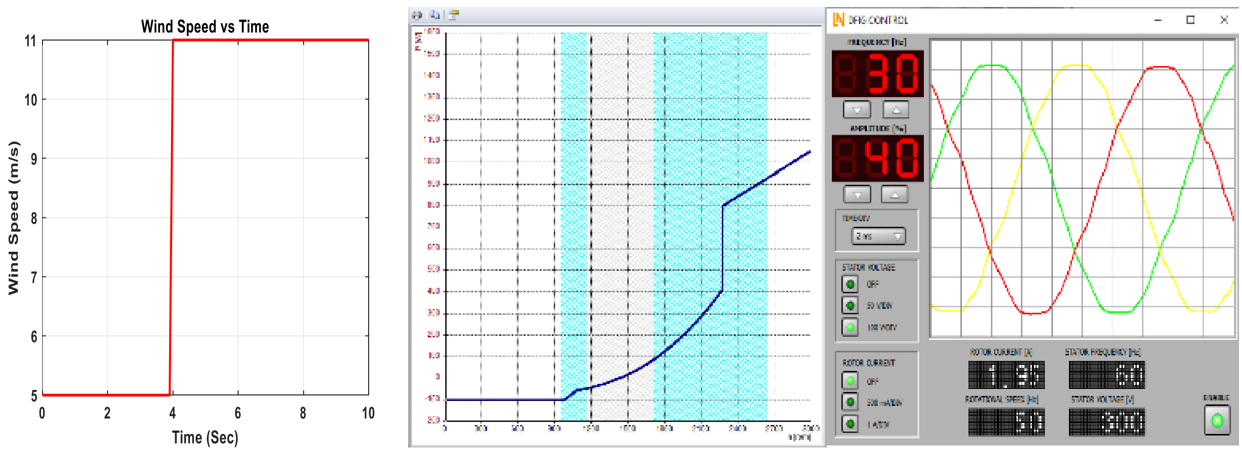

(a) (b) (c)

Figure. 11 Real-time DFIG wind turbine performance analysis: (a) Wind speed profile, (b) Rotor response of DFIG, and (c) The generated voltage

Received: April 13, 2025. Revised: May 20, 2025.

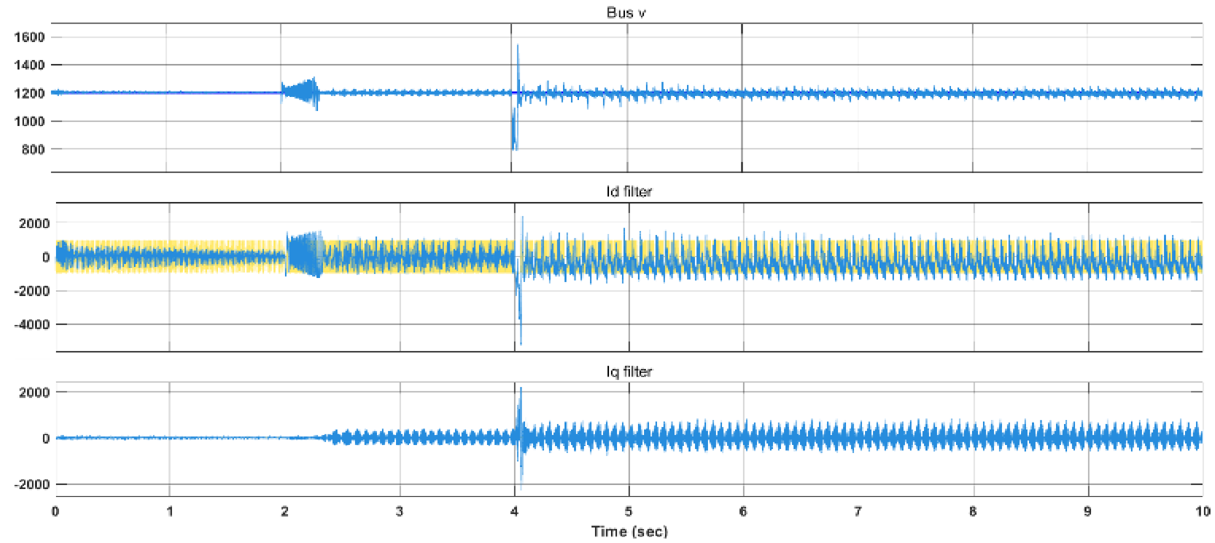

Figure. 12 Wind turbine characteristics using PSO-Fuzzy controller

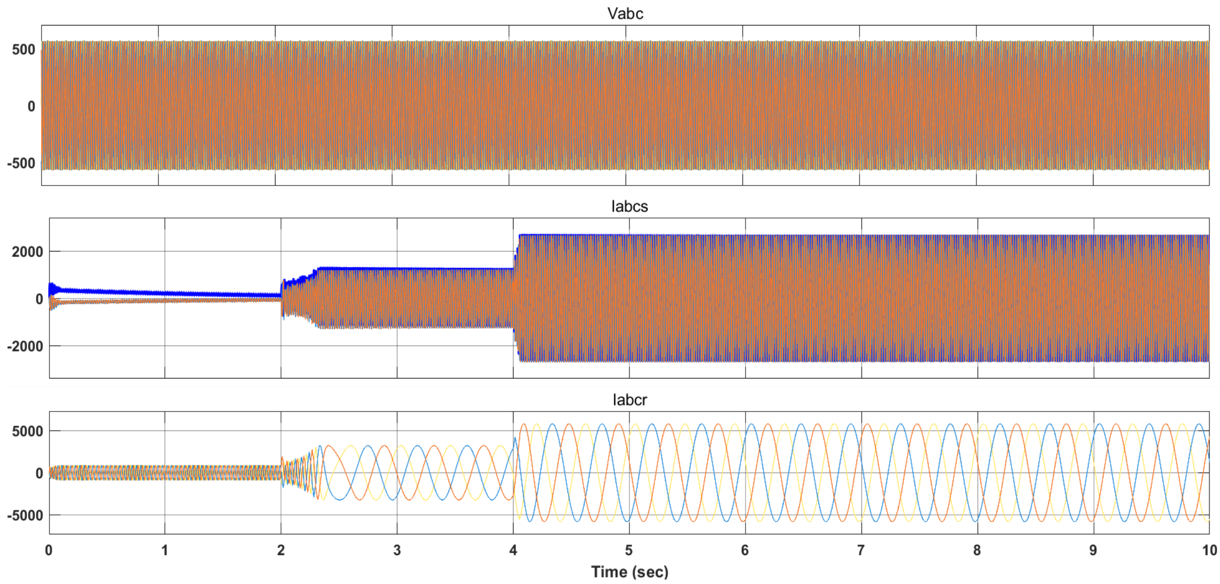

Figure. 13 Wind turbine characteristics using PSO-PI controller

Fig. 12 shows the voltage, stator, and rotor current based on the PSO-Fuzzy controller. It displays the source voltage generated by the inverter and the source and rotor currents over Time. The current source is integral to the power exchange between a DFIG and a grid. Monitoring a source current is vital for assessing the system's impact on the grid, as excessive currents can lead to grid instability or damage to components. Fig. 13 shows wind turbine characteristics using the PSO-PI controller. It shows the voltage output, stator current, and rotor current. Each three-phase electrical energy across the generator terminals is relatively constant throughout the period, indicating the stability of the system voltage, which is necessary for connecting the turbine to the electrical grid. Stator current I_{abcs} At the start of the operation, the current is low, then increases significantly after a particular moment (approximately three seconds), which may indicate that the generator has entered its entire operating range when loaded. Some fluctuations may be observed, which may be a result of the power control adjustment process. Rotor current I_{abcr} shows how the rotor current changes over time.

At the start of operation, the current is low and then gradually increases as loads increase or torque is controlled. The current appears to reach a steady state after approximately 4 seconds, indicating that the control system has adjusted to achieve optimal power generation.

Fig. 14 shows voltage and d-q current based on the PSO-ANFIS controller. The figure illustrates the source and rotor side currents for the PSO-ANFIS controller and the voltage source-based PSO-ANFIS controller. Fig. 14a shows the source current with FLC. With FLC,the source current i_s tends to have

Received: April 13, 2025.   Revised: May 20, 2025.

reduced fluctuations and harmonics, indicating a superior capability of FLC in maintaining the excellence of power fed into a network. FLC is expected to result in a more harmonious and less distorted current waveform. Fig. 14b shows the rotor side current with FLC. Employing FLC results in iabcr that exhibits minimal fluctuations, suggesting that FLC effectively regulates the rotor currents. This is crucial for reducing stress on rotor windings and converters, highlighting the adaptive nature of FLC in efficiently handling system dynamics.

Fig. 14c shows the source voltage with the PSO-ANFIS controller. While FLC does not directly control source voltage, improved stability and performance of the overall DFIG system under FLC indirectly contribute to a more stable source voltage profile, reflecting the holistic benefits of fuzzy control.

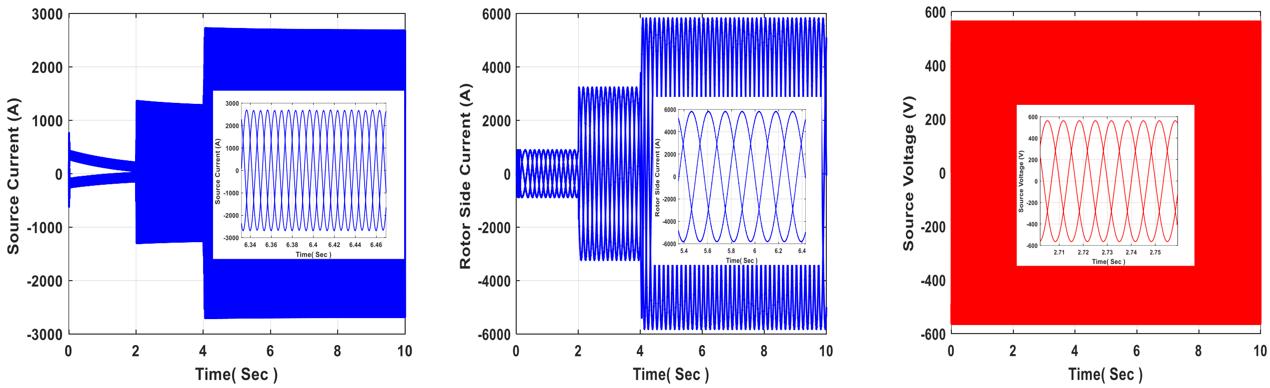

(a) (b) (c)

Figure. 14 Current and voltage waveforms are based on the PSO-ANFIS controller: (a) The source current, (b) The rotor current, and (c) The source voltage

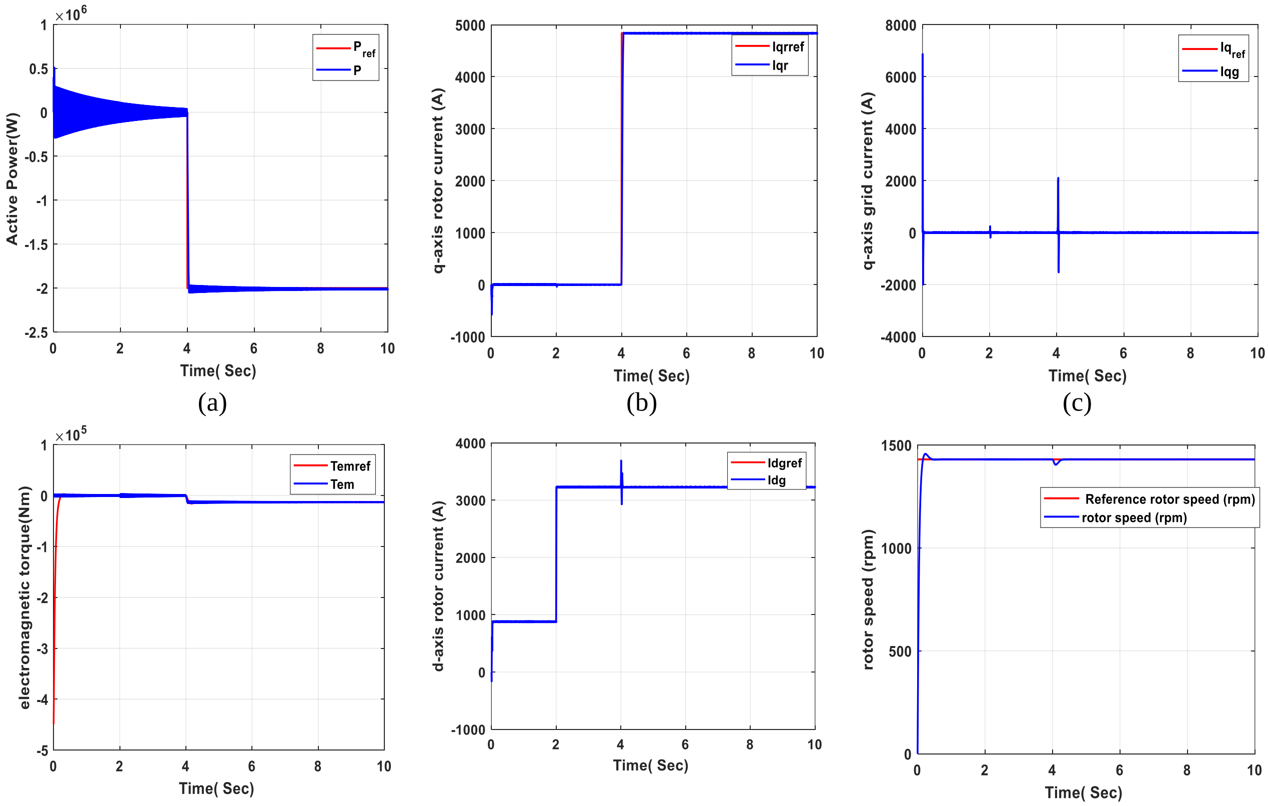

(a) (b) (c)

(d) (e) (f)

Figure. 15 A system response :(a) Active power–time response, (b) q-axis of rotor current response, (c) q-axis of grid current response, (d) Electromagnetic torque time response, (e) The time response of the d-axis rotor current, and (f) The time response of the rotor speed

Received: April 13, 2025. Revised: May 20, 2025.

Fig. 15 shows the system response. Fig. 15a shows the active power use of the PSO-ANFIS controller. With PSO-ANFIS, the controller reduces settling time and overshooting. This likely results from the FLC's rule-based nature, which provides efficient and precise power control and grid synchronization under varying wind settings. Fig. 15b shows the q-axis rotor current with the PSO-ANFIS controller. The control over the rotor current is i_{qr}, bringing it rapidly and smoothly in line with i_{qrr}.

The controller is adept at reducing transient fluctuations and settling the system to a steady state with minimal errors. This indicates an efficient and responsive control strategy that ensures precise reactive power management within the rotor circuit. There are no significant differences between the stator and rotor DQ currents due to this variation in speed as shown in Figs. 15c and. It can be observed from these figures that the q-axis represents the response to the variable winding speed, and the d-axis currents have oscillated about the zero axis. Fig. 15e illustrates the rotor current along the D-axis. This plot compares the reference d-axis rotor current. i_{drr} with real d-axis rotor current i_{dr} The d-axis rotor current controls the active power exchanged between the DFIG and the grid. An effective PI controller will facilitate the i_{dr} closely track $i.$ sub d r rely. The difference between these two lines can indicate the controller's performance; more significant gaps may suggest potential issues in power control and may necessitate controller. Fig. 15f is expected to demonstrate rapid and precise tracking of the reference rotor speed. The controller's agility in adapting to changes ensures fast response, minimal overshoot, and superior steady-state monitoring, which are essential for maximizing energy capture in variable wind conditions.

6.3 The optimal parameters of the controller

Based on multivariable state feedback and DQ-reference frame theory, these controllers stabilize the DC connection voltage and manage the stator's reactive power for optimal wind energy harvesting [32, 33]. However, the results show lower transient responses and dynamic performance, yet the system adapts effectively under various operating conditions through feedforward and feedback components. The simulation results depend on the optimal parameters exposed in Table 7. The transient response analysis during the startup of the DFIG or changes in the load. In DFIG, the damping ratio zeta and natural frequency omega are derived from second-order systems. The damping ratio ζ determines the system's ability to reduce oscillations during transition states.

Table 7. The optimal controller parameters are based on the PSO algorithm

Parameter	**Symbol**	**Value**
Proportional Gain (d-axis)	kpid	1.2531
Proportional Gain (q-axis)	kpiq	1.2531
Integral Gain (d-axis)	kiid	1.976e+03
Speed Proportional Gain	kpv	3000
Speed Integral Gain	kiv	3.433e+04
Grid side Proportional Gain	Kpg	0.0016
Grid side Integral Gain	Kqfg	0.0016
DC Voltage Proportional Gain	kpvdc	220000
Integral Gain for Vdc	kivdc	10000
Proportional Gain for the controller	kpf	0.0013
Derivative Gain for the controller	kdf	0.58

6.4 The dynamic behavior of DFIG

At the same time, the natural frequency ω_{n} expresses the system's self-oscillatory response associated with energy storage. In this context, the expected frequency ω_{n} is related to the frequency of the electrical system resulting from the interaction of a rotating magnetic field between the stator and the rotor, and is given by

$$\omega_{\mathrm{n}} = \sqrt{\frac{K_{\mathrm{e}}}{J}} \tag{43}$$

where K_{e} is the electromechanical constant, and J is the instant of inertia of the rotor part, the damping ratio ζ depends on the damping currents or the resistance to oscillations resulting from the interactions between the stator and rotor. It is given by

$$\zeta = \frac{B}{(2\sqrt{K_{\mathrm{e}} \cdot J})} \tag{44}$$

where B represents the damping coefficient, which is influenced by internal resistance and eddy current losses. The parameters ω_{n} and ζ in the second-order system, determine the generator's dynamic response under transient conditions such as load variations and startup [26, 27]. The natural frequency ω_{n} dictates the oscillation speed following a disturbance, while the damping ratio ζ regulates the rate at which these oscillations decay and how quickly the generator stabilizes. The system's response is characterized based on ζ as given in Table 8.

Table 8. The behavior systems based on ζ

Case	**ζ value**	**Generator Behavior**
Critically Damped	$\zeta = 1$	The generator achieves a steady state in the shortest time without producing oscillations.
Underdamped	$0 < \zeta < 1$	The generator undergoes oscillations before eventually stabilizing.
Overdamped	$\zeta > 1$	The generator reaches a steady state without oscillating.
Undamped	$\zeta = 0$	The generator continues to oscillate indefinitely without diminishing.

The dynamic behavior of the second order in DFIG can be represented as:

$$\Theta(s) = \left[\frac{{\omega_n}^2}{(s^2 + 2\zeta\omega_n s + {\omega_n}^2)}\right] \cdot \left(\frac{T_m}{s}\right) \quad (45)$$

where the mechanical torque is applied to a rotor (T_m) is the, $\Theta(s)$ is the angular displacement of the rotor.

Use ω_n and ζ To accurately estimate the generator's performance and optimize it for specific applications, Fig. 16 shows the DFIG's rotor response, illustrating the second-order time response. Table 9 compares the proposed controller's performance. The comparison shows that using ANFIS to adjust time, settling time, and set time as the maximum overshoot will modify these parameters.

7. Conclusions

This research presented a hybrid control strategy that combines a PSO-tuned PI controller, a FLC fuzzy controller, and an ANFIS. This strategy aimed to improve the dynamic performance of a DFIG-based wind power system. These models were simulated in MATLAB/Simulink and a real-time system, ensuring their applicability in real-world scenarios.

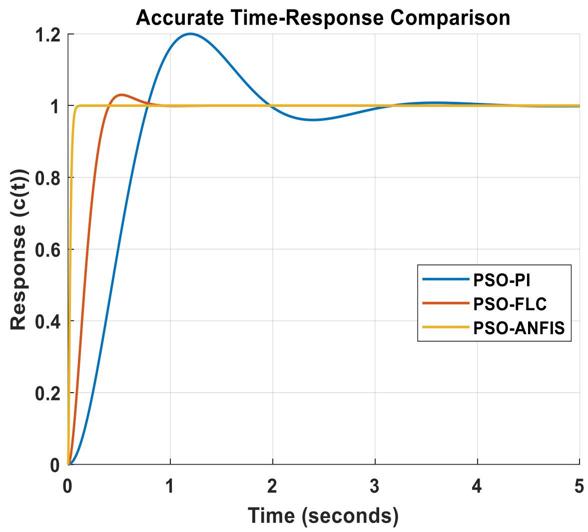

Figure. 16 Rotor response of DFIG: Time response of the second-order system

Table 9. Compression of the performance DFIG wind turbine

Perfor-mance Metric	**PI**	**Fuzzy**	**PSO-PI**	**PSO-FLC**	**PSO-ANFIS**	**Remarks**
Rise Time (sec)	0.89	0.72	0.61	0.201	0.12	PSO-ANFIS combines PSO's optimization capabilities with ANFIS's adaptive learning, resulting in even faster response times.
Settling Time (sec)	1.25	0.95	0.721	0.24	0.16	PSO-ANFIS enhances settling time by leveraging PSO for parameter optimization and ANFIS for dynamic adaptability.
Oversho-ot (%) RPM	28	27	22	0	0	PSO-ANFIS effectively reduces overshoots to zero, utilizing PSO's optimization to fine-tune ANFIS parameters for smoother transitions.
Steady-State Error (RPM)	3.2	2.61	2.47	0.4	0.15	PSO-ANFIS achieves the lowest steady-state error, as PSO optimizes ANFIS to handle system variations for enhanced stability adaptively.
Ripple (A)	14.4	8.2	5.3	2.4	1.5	PSO-ANFIS produces minimal ripples by optimizing ANFIS's ability to manage uncertainties, yielding smooth control outputs with high precision.
THD%	6.8	4.6	4.21	1.42	0.9	PSO-ANFIS achieves the lowest THD, as PSO optimizes ANFIS parameters for purer output signals by adapting to real-time patterns.

The optimum design of DFIG investigated the influence of main manufacturing parameters, such as the number of slots and stator resistance, in addition to variable wind speed conditions. A developed, efficient control model explicitly focuses on enhancing the performance of a DFIG by utilizing the energy from a wind turbine. The system adapts to variable-speed operation, ensuring improved efficiency and stability.

This study comprehensively analyzes, models, and evaluates the proposed control strategy, developing an efficient control paradigm for a DFIG-based (variable-speed) turbine energy system integrated with the grid. Simulation results significantly improved compared to conventional controllers such as PI and FLC alone. The reported values represent the mean and standard deviation calculated from 10 independent simulation runs under variable wind profiles. The PSO-ANFIS hybrid controller achieved a lower total harmonic distortion (THD) of 0.9%. Overshooting was also eliminated, reaching 0%. The steady-state error was reduced to 0.15 RPM. The response time was reduced to 0.12 seconds, and the settling time to 0.16 seconds. These results confirm the effectiveness of the proposed approach and its high adaptability to wind speed changes. Thus, this work supports more intelligent and more stable integration of renewable energy systems.

Conflicts of Interest

Declare conflicts of interest or state, “The authors declare no conflict of interest.” Authors must identify and declare any personal circumstances or interests perceived as inappropriately influencing the representation or interpretation of reported research results.

Author Contributions

Conceptualization, Abood and Annamalai; methodology, Abood and Khalid; software, Abood; validation, Abood, Annamalai, and Chouikha; formal analysis, Abood; investigation, Al-Zuhairi; resources, Khalid; data curation, Abood; writing—original draft preparation, Abood and Khalid; writing—review and editing, Annamalai, Chouikha and Al-Zuhairi; visualization, Abood.

Acknowledgments

This work was supported in part by NSF award #2219611 (HBCU-RISE: Enhancing Cybersecurity Research and Education Infrastructure at Prairie View A&M University) and a Panther RISE grant.

References

[1] M. I. C. Quispe, F. V. C. Cárdenas and E. C. Quispe, “Method for Steady State Analysis of Doubly Fed Induction Generator”, *IEEE ANDESCON*, pp. 1-7, 2018.

[2] I. C. EWG1, “Wind power plants with DFIG”, *Lucas Nülle*, Cologne, Germany, 2018.

[3] K. Okedu, “Performance of DFIG and PMSG Wind Turbines”, *Boca Raton*, FL: CRC Press, 2023.

[4] M. Ferrari, E. C. Piesciorovsky and L. M. Tolbert, “Real-Time Emulation of Grid-Connected DFIG Wind Energy System with Model Validation from Sub-synchronous to Hyper-synchronous Operation under Unbalanced Conditions”, *IEEE Power & Energy Society General Meeting*, pp. 01-05, 2022.

[5] B. Garkki and S. Revathi, “Direct speed fractional order controller for maximum power tracking on DFIG-based wind turbines during symmetrical voltage dips”, *International Journal of Dynamics and Control*, Vol. 12, No. 1, pp. 211-226, 2024.

[6] K. F. Sayeh, S. Tamalouzt, Y. Sahri and S. Sofia Lalouni Belaid, “Artificial intelligence-based direct power control for power quality improvement in a WT-DFIG system via neural networks: Prediction and classification techniques”, *Elsevier.Journal of the Franklin Institute*, pp. 358-383, 2025.

[7] Y. Zhang, J. Chen and L. Wei, “Artificial neural network-based predictive direct control for wind turbine generators: A frequency-speed optimization approach”, *International Journal of Renewable Energy Research*, pp. 115-123, 2024.

[8] H. Liu, X. Wang and R. Zhao, “A hybrid fuzzy-PSO control strategy for wind energy systems using DFIG: Enhancing dynamic tracking and reducing steady-state error”, *Energy Reports*, p. 2459-2470, 2025.

[9] E. Rajendran, R. Sridevi and N. R. Vallarasu, “Artificial Intelligence-RNN Control Of Double Fed Induction Generator-Based Wind Energy Conversion System”, In: *Proc. of International Conference on Energy, Materials and Communication Engineering (ICEMCE)*, 2024.

[10] C. Dardabi, D. A. H. Chojaa, H. Aziz, A. Mouradi, M. A. Mossa, A. Y. Abdelaziz and T. A. H. Alghamdi, “Enhancing the control of

doubly fed induction generators using artificial neural networks in the presence of real wind profiles", *Public Library of Science (PLOS)*, pp. 1-10, 2024.

[11] X. Li, K. Shi, L. Han, C. J. W. Sun and Z. Peng, "A looped-type functional for non-fragile fuzzy sampled-data control of doubly fed induction generator-based wind energy conversion systems with failures", *Engineering Applications of Artificial Intelligence*, Vol. 142, p. 109812, 2025.

[12] R. Yang, S. Peng and G. Yao., "A multi-modal feature combination mechanism for identification of harmonic load in distribution networks based on artificial intelligence models", *International Journal of Electrical Power and Energy Systems*, Vol. 166, p. 110519, 2025.

[13] K. F. Sayeh, S. Tamalouzt, Y. Sahri, S. L. Belaid and A. Bekhiti., "Artificial intelligence-based direct power control for power quality improvement in a WT-DFIG system via neural networks: Prediction and classification techniques", *Journal of the Franklin Institute*, Vol. 362, No. 1, p. 107401., 2025.

[14] W. Ma, H. Shi, C. Wang and B. Chen, "Variational Bayesian EnKF with generalized mixture Corr entropy loss-based dynamic state estimation for DFIG", *Signal Processing*, Vol. 230, p. 109838., 2025.

[15] C. Sreenu, G. Mallesham, T. C. Shekar and S. R. Salkuti, "High Gain Quasi Z-Source Converters with Artificial Bee Colony Control for Grid-Integrated Solar-Wind Energy Sources", *Green Energy and Intelligent Transportation 100264*, 2025.

[16] A. Loulijat, A. Hilali, M. Makhad, H. Chojaa, N. Ababssi and M. A. Mossa, "Low-voltage ride-through capability of DFIG-based WECS improved by nonlinear backstepping controller synthesized in novel power state model", *e-Prime - Advances in Electrical Engineering, Electronics and Energy*, pp. 1-21, 2025.

[17] S. Sanati and M. Azzouz, "A new inrush current detection for collector transformers' differential protection in DFIG-based wind farms", *Electric Power Systems Research*, Vol. 225, p. 109766, 2023.

[18] O. A.-Z. Al-Khaldi, "Rotor current control design for DFIG-based wind turbine using PI, FLC, and fuzzy PI controllers", In: *Proc, of IEEE, International Conference on Electrical and Computing Technologies and Applications (ICECTA)*, pp. 1-6, 2019.

[19] A. E. Amorim, F. D. Oliveira and D. S. Simonetti, "A new hybrid multilevel back-to-back converter for doubly fed induction generator-based wind turbines' fault supportability", *International Transactions on Electrical Energy Systems*, Vol. 31, No. 3, p. e12793, 2021.

[20] N. H. Nam, "Modeling, algorithm control, and simulation of a variable-speed doubly fed induction generator in grid-connected operation", *International Workshop on Electric Drives: Improvement in the Efficiency of Electric Drives (IWED)*, pp. 1-5, 2019.

[21] M. Zerzeri, F. Jallali and A. Khedher, "Robust FOC Analysis of a DFIM using an SMFO: Application to Electric Vehicles", In: *Proc. of IEEE, International Conference on Signal, Control, and Communication (SCC)*, pp. 250-255, 2019.

[22] I. Naveed, G. Zhao, Z. Yamin and W. Gul., "Steady State Performance Analysis of DFIG with Different Magnetizing Strategies in a Pitch-Regulated Variable Speed Wind Turbine", In: *Proc. of IEEE, International Conference on Power and Energy Engineering (ICPEE)*, pp. 174-179, 2020.

[23] M. Sharawy, A. A. Shaltout, N. Abdel-Rahim, O. E. M. Youssef and M. A. Al-Ahmar., "Simplified Steady State Analysis of Stand-Alone Doubly Fed Induction Generator", In: *Proc. of IEEE, International Middle East Power Systems Conference (MEPCON)*, pp. 246-251, 2021.

[24] G. T. Arjun, N. S. Jyothi and V. S. Neethu, "Vector Control of Doubly fed Induction Machine for an Electric Vehicle Application", In: *Proc. of IEEE, International Conference on Recent Trends on Electronics, Information, Communication & Technology (RTEICT)*,, pp. 784-787, 2021.

[25] A. Fathy, A. G. Alharbi, S. Alshammar and H. M. Hasanien, "Archimedes optimization algorithm-based maximum power point tracker for wind energy generation system", *Ain Shams Engineering Journal*, Vol. 13, No. 2, p. 101548, 2022.

[26] L. Wu, H. Liu, J. Zhang, Chenyu Liu, Y. Sun, Z. Li and J. Li., "Identification of control parameters for converters of doubly fed wind turbines based on hybrid genetic algorithm.", *Processes*, Vol. 10, No. 3, p. 567, 2022.

Received: April 13, 2025. Revised: May 20, 2025.

[27] D. R. Karthik, S. M. Kotian and N. S. Manjarekar, "An accurate method for steady-state initialization of doubly fed induction generator", In: *Proc. of IEEE International Conference on Power Electronics, Smart Grid, and Renewable Energy*, pp. 1-6, 2022.

[28] B. Aljafari, P. Stephenraj, V. J., I. and R. Singh Rassiah, "Steady-state modeling and performance analysis of a wind turbine-based doubly fed induction generator system with rotor control", *Energies*, Vol. 15, No. 9, p. 3327, 2022.

[29] L. Yang, G. Y. Yang, Z. Xu, Z. Y. Dong and Y. Xue., "Optimal controller design of a wind turbine with doubly fed induction generator for minor signal stability enhancement.", *Wind Power Systems: Applications of Computational Intelligence,* pp. 167-190, 2010.

[30] D. Xu, F. Blaabjerg, W. Chen and N. Zhu, "Advanced control of doubly fed induction generator for wind power systems", *Halifax*, Nova Scotia,: John Wiley & Sons, 2018.

[31] N. Karakasis, E. Tsioumas, N. Jabbour, A. M. Bazzi and C. Mademlis., "Optimal efficiency control in a wind system with a doubly fed induction generator", *IEEE Transactions on Power Electronic*s, Vol. 34, No. 1, pp. 356-368, 2018.

[32] S. Vadi, F. B. Gürbüz, R. Bayindir and E. Hossain, "Design and simulation of a grid-connected wind turbine with a permanent magnet synchronous generator", In: *Proc. of IEEE, 8th International Conference on Smart Grid*, pp. 169-175, 2020.

[33] A. I. Wagan and M. M. Shaikh, "A new method of optimization algorithm inspired by human dynasties with an application to the wind turbine microsite problem", *Applied Soft Computing*, 2020.